
Personalized Federated Dictionary Learning for Modeling Heterogeneity in Multi-site fMRI Data

Yipu Zhang*

Tulane Center for Biomedical Informatics and Genomics
School of Medicine, Tulane University
New Orleans, LA 70112, USA

Chengshuo Zhang

School of Energy and Electrical Engineering
Chang'an University
Xi'an 710064, China

Ziyu ZHou

Department of Computer Science
Tulane University
New Orleans, LA 70112, USA

Gang Qu

Department of Biomedical Engineering
Tulane University
New Orleans, LA 70112, USA

Hao Zheng

State University of New York at Oswego
USA
zheng.hao@oswego.edu

Yuping Wang

Department of Biomedical Engineering
Tulane University
New Orleans, LA 70112, USA

Hui Shen

Tulane Center for Biomedical Informatics and Genomics
School of Medicine, Tulane University
New Orleans, LA 70112, USA

Hongwen Deng

Tulane Center for Biomedical Informatics and Genomics
School of Medicine, Tulane University
New Orleans, LA 70112, USA

Abstract

Data privacy constraints pose significant challenges for large-scale neuroimaging analysis, especially in multi-site functional magnetic resonance imaging (fMRI) studies, where site-specific heterogeneity leads to non-independent and identically distributed (non-IID) data. These factors hinder the development of generalizable models. To address these challenges, we propose Personalized Federated Dictionary Learning (PFedDL), a novel federated learning framework that enables collaborative modeling across sites without sharing raw data. PFedDL performs independent dictionary learning at each site, decomposing each site-specific dictionary into a shared global component and a personalized local component. The global atoms are updated via federated aggregation to promote cross-site con-

*Corresponding author.

sistency, while the local atoms are refined independently to capture site-specific variability, thereby enhancing downstream analysis. Experiments on the ABIDE dataset demonstrate that PFedDL outperforms existing methods in accuracy and robustness across non-IID datasets.

1 Introduction

Functional connectivity networks (FCNs), derived from resting-state functional magnetic resonance imaging (fMRI), capture temporal correlations between anatomically distinct brain regions and are widely used to characterize neural dysfunctions in neurological and psychiatric disorders [1][2][3]. To enhance statistical power and improve generalizability, federated learning (FL) has been introduced as a promising approach that enables collaborative model training across decentralized sites without sharing raw data [4][5]. However, variations in imaging protocols, scanner hardware, and subject demographics across sites result in non-independent and identically distributed (non-IID) data, which can significantly degrade model performance and hinder generalization. Although recent approaches have incorporated domain adaptation techniques into FL frameworks to mitigate distributional shifts between sites [6][7], these methods often rely on complex deep learning architectures with limited interpretability, an important limitation in clinical neuroimaging, where transparency and explainability are essential [8].

Dictionary learning (DL) offers a more interpretable alternative by modeling each sample as a sparse combination of basis atoms. This approach supports dimensionality reduction while preserving key discriminative features. In fMRI studies, DL has been used to isolate individual variability and uncover biologically significant patterns [9]. However, conventional DL assumes centralized and homogeneous data, which makes it unsuitable for federated neuroimaging applications that involve heterogeneity and privacy constraints [10][11].

To this end, we propose Personalized Federated Dictionary Learning (PFedDL), a novel framework that combines orthogonal sparse dictionary learning with personalized federated optimization. By decomposing the dictionary into global and local components, PFedDL facilitates interpretable modeling of shared and site-specific patterns while ensuring data privacy. This unified approach bridges the gap between interpretable sparse modeling and the decentralized, heterogeneous nature of multi-site neuroimaging analysis. Our key contributions are as follows:

- Personalized federated modeling: PFedDL decomposes each site-specific dictionary into global and local components, aggregating only the global atoms across sites to capture shared structures while preserving local specificity.
- Distribution-aware personalization: Each site learns a model tailored to its own data distribution, enhancing prediction performance under non-IID conditions.
- Cross-site dictionary alignment: A dictionary alignment mechanism is introduced to maintain consistent atom ordering across site-specific dictionaries, enhancing interpretability and training stability.
- Sparse and orthogonal coding: By enforcing sparsity and orthogonality constraints in DL, PFedDL captures low-dimensional, discriminative representations that enhance accurate disease analysis.

2 Method

2.1 Dictionary Learning

Dictionary learning [12] is a powerful technique for extracting sparse representations from high-dimensional data by learning a set of representative basis elements, commonly called atoms. It has been widely applied in areas such as feature extraction, signal compression, and pattern recognition [13][14][15]. The key idea is to approximate each data sample as a sparse linear combination of dictionary atoms, resulting in a sparse representation matrix \mathbf{S} . Formally, the sparse DL is posed as the following optimization:

$$\min_{\mathbf{D}, \mathbf{S}} \|\mathbf{X} - \mathbf{D}\mathbf{S}\|_F^2 + \lambda_1 \|\mathbf{S}\|_1 \quad (1)$$

where $X \in R^{d \times n}$ denotes the observed data matrix, with each column representing a sample; $D \in R^{d \times k}$ is the dictionary matrix to be learned, consisting of k atoms (each column is an atom); and $S \in R^{k \times n}$ is the sparse coefficient matrix that represents the data as a linear combination of dictionary atoms. $\|\cdot\|_F$ denotes the Frobenius norm, $\|\cdot\|_1$ represents the ℓ_1 -norm [16][17], the regularization parameter $\lambda_1 > 0$ controls the strength of the sparsity constraint. The optimization problem in Eq. (1) is typically solved using an alternating minimization strategy. Specifically, the sparse coefficients S are updated while keeping the dictionary D fixed, and vice versa, the dictionary D is updated while keeping the sparse coefficients S fixed.

2.2 PFedDL

Federated learning in neuroimaging often contends with non-IID data, where client-specific variations, arising from differences in scanner protocols, demographic distributions, and acquisition conditions, result in significant heterogeneity across sites. In such settings, a single global dictionary is inadequate because it cannot simultaneously reflect shared structure and site-specific nuances, thereby limiting generalizability and degrading site-level performance.

To overcome this limitation, we introduce personalized federated dictionary learning (PFedDL). Figure 1 presents the overall framework of the proposed PFedDL method. Specifically, PFedDL decomposes the dictionary of each site into two components: a global dictionary and a local dictionary. The global dictionary models structural patterns common to all sites, enhancing cross-site generalization. The local dictionary captures site-specific variations, allowing the model to better adapt to the unique distribution of each individual site.

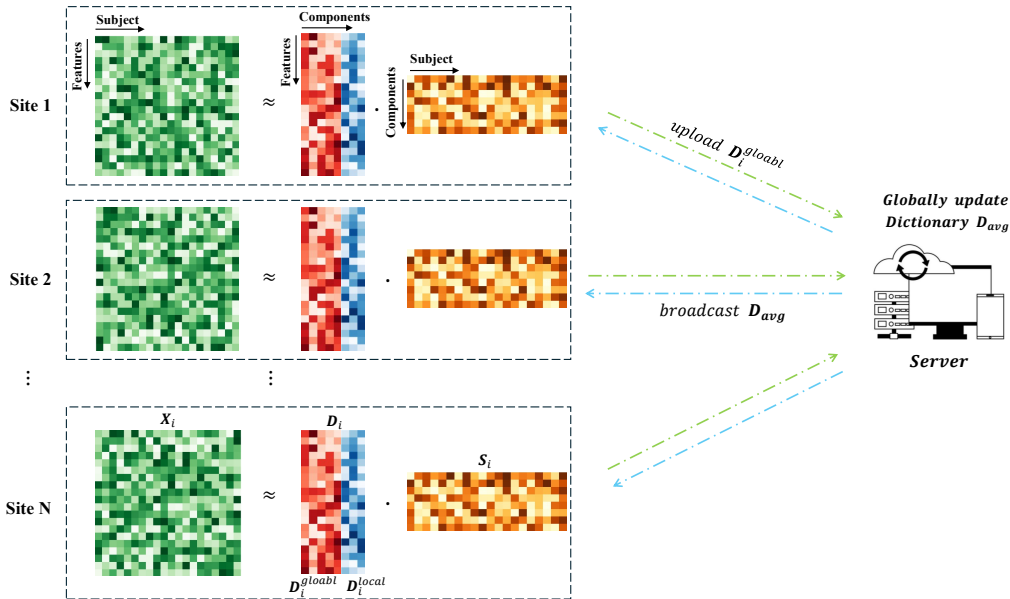


Figure 1: The framework of PFedDL

During training, each site jointly optimizes both dictionary components locally. However, only the global dictionary is transmitted to the server for aggregation, while local dictionaries remain on-device to preserve privacy and maintain site-specific heterogeneity. This dual-component structure enables PFedDL to balance global consistency with local adaptability, making it especially suitable for decentralized neuroimaging applications where interpretability and site-level heterogeneity are essential. To further disentangle the global and local components within each site, we impose orthogonality constraints that encourage linear independence among dictionary atoms. This promotes a clearer separation between shared and site-specific representations. Consequently, PFedDL can more effectively decouple the global and local components, providing a solid theoretical foundation for cross-site dictionary alignment. However, since each site trains on non-IID data, the global dictionaries can still become misaligned across clients. From a theoretical perspective, these discrepancies

can be viewed as equivalence class transformations, such as permutations or rotations of dictionary atoms, which highlight the necessity for explicit alignment across clients.

2.3 Cross-Client Atom Alignment

Due to privacy constraints and preserving raw data sharing, aligning dictionaries independently trained on non-IID data becomes a non-trivial task. Theoretically, these inconsistencies can be modeled as an equivalence class problem.

Let $\mathbf{P} \in \mathbb{R}^{k \times k}$ be an orthogonal matrix satisfying $\mathbf{P}\mathbf{P}^T = \mathbf{I}$, where \mathbf{I} is the identity matrix. If two dictionaries satisfy $\mathbf{D}_2 = \mathbf{D}_1\mathbf{P}$, we denote $\mathbf{D}_1 \sim \mathbf{D}_2$, indicating that they belong to the same equivalence class. Even when two clients have identical data, they may learn \mathbf{D}_1 and $\mathbf{D}_2 = \mathbf{D}_1\mathbf{P}$ since:

$$\mathbf{D}_1\mathbf{S}_1 = \mathbf{D}_1\mathbf{P}\mathbf{P}^T\mathbf{S}_1 = \mathbf{D}_2\mathbf{S}_2 \quad (2)$$

Thus, the reconstruction capabilities of \mathbf{D}_1 and \mathbf{D}_2 are functionally equivalent, even though the dictionaries themselves are not uniquely identifiable. The matrix \mathbf{P} may represent a composition of transformations, including rotation, rescaling, and sign permutation. To address these, rescaling is typically mitigated by enforcing unit-norm constraints on dictionary atoms. Rotation effects are suppressed by the sparsity constraints imposed on the coefficient matrix \mathbf{S} . Signed permutations remain the primary challenge and are addressed using the following theoretical result.

The following theorem further demonstrates that in certain iterative optimization processes, if the initial dictionaries satisfy the equivalence relation $\mathbf{D}_2 = \mathbf{D}_1\mathbf{P}$, then this equivalence is preserved throughout all iterations, that is, $\mathbf{D}_2^t = \mathbf{D}_1^t\mathbf{P}$ for all t . This property establishes a theoretical foundation for the subsequent alignment strategy and consistency modeling.

Theorem(Permutation Invariance): Let $\mathbf{D}_0 \in \mathbb{R}^{d \times k}$ be an initial dictionary, and $\mathbf{S}_0 \in \mathbb{R}^{k \times n}$ be an initial sparse code. For a given permutation matrix $\mathbf{P} \in \mathbb{R}^{k \times k}$ satisfying $\mathbf{P}\mathbf{P}^T = \mathbf{I}$ (where \mathbf{I} is the identity matrix) and given constants $\eta, \lambda, \varepsilon > 0$, define $\tilde{\mathbf{D}}_0 = \mathbf{D}_0\mathbf{P}$, $\tilde{\mathbf{S}}_0 = \mathbf{P}^T\mathbf{S}_0$. Consider the following iterative updates applied to both $(\mathbf{D}_k, \mathbf{S}_k)$ and $(\tilde{\mathbf{D}}_k, \tilde{\mathbf{S}}_k)$:

$$\mathbf{S}_{k+1} = \text{SoftThreshold} \left(\mathbf{S}_k - \eta \left[\mathbf{D}_k^T (\mathbf{D}_k \mathbf{S}_k - \mathbf{X}) \right], \varepsilon \right) \quad (3)$$

$$\text{SoftThreshold}(x, \lambda) = \text{sign}(x) \max(|x| - \lambda, 0) \quad (4)$$

$$\mathbf{D}_{k+1} = \mathbf{D}_k - \eta \left[(\mathbf{D}_k \mathbf{S}_{k+1} - \mathbf{X}) \mathbf{S}_{k+1}^T + \lambda \mathbf{D}_k (\mathbf{D}_k^T \mathbf{D}_k - \mathbf{I}) \right] \quad (5)$$

Then, for all $k \geq 0$, it holds that $\mathbf{D}_k = \mathbf{D}_k\mathbf{P}$, $\mathbf{S}_k = \mathbf{P}^T\mathbf{S}_k$. The proof is presented as follows.

Proof We use the proof by induction on k . When $k=0$, by definition $\tilde{\mathbf{D}}_0 = \mathbf{D}_0\mathbf{P}$, $\tilde{\mathbf{S}}_0 = \mathbf{P}^T\mathbf{S}_0$. Assume the theorem holds for some $k \geq 0$. For $\tilde{\mathbf{S}}_{k+1}$,

$$\tilde{\mathbf{S}}_{k+1} = \text{SoftThreshold} \left(\mathbf{P}^T \mathbf{S}_k - \eta \left[\mathbf{P}^T \mathbf{D}_k^T (\mathbf{D}_k \mathbf{P} \mathbf{P}^T \mathbf{S}_k - \mathbf{X}) \right], \varepsilon \right) \quad (6)$$

$$= \text{SoftThreshold} \left(\mathbf{P}^T \mathbf{S}_k - \eta \left[\mathbf{P}^T \mathbf{D}_k^T (\mathbf{D}_k \mathbf{S}_k - \mathbf{X}) \right], \varepsilon \right) \quad (7)$$

Notice by definition of soft-threshold, since permutation only changes the position of the values in \mathbf{V} , but not the values themselves, the following holds for any matrix \mathbf{V} ,

$$\text{SoftThreshold}(\mathbf{P}^T \mathbf{V}, \varepsilon) = \mathbf{P}^T \text{SoftThreshold}(\mathbf{V}, \varepsilon) \quad (8)$$

Thus,

$$\text{SoftThreshold} \left(\mathbf{P}^T \mathbf{S}_k - \eta \left[\mathbf{P}^T \mathbf{D}_k^T (\mathbf{D}_k \mathbf{S}_k - \mathbf{X}) \right], \varepsilon \right) = \mathbf{P}^T \mathbf{S}_{k+1} \quad (9)$$

Combining the above results yields $\tilde{\mathbf{S}}_{k+1} = \mathbf{P}^T \mathbf{S}_{k+1}$ for \mathbf{D}_{k+1} ,

$$\begin{aligned} \tilde{\mathbf{D}}_{k+1} &= \tilde{\mathbf{D}}_k - \eta \left[(\tilde{\mathbf{D}}_k \tilde{\mathbf{S}}_{k+1} - \mathbf{X}) \tilde{\mathbf{S}}_{k+1}^T + \lambda \tilde{\mathbf{D}}_k (\tilde{\mathbf{D}}_k^T \tilde{\mathbf{D}}_k - \mathbf{I}) \right] \\ &= \mathbf{D}_k \mathbf{P} - \eta \left[(\mathbf{D}_k \mathbf{P} \mathbf{P}^T \mathbf{S}_{k+1} - \mathbf{X}) \mathbf{S}_{k+1}^T \mathbf{P} + \lambda \mathbf{D}_k \mathbf{P} (\mathbf{P}^T \mathbf{D}_k^T \mathbf{D}_k \mathbf{P} - \mathbf{I}) \right] \\ &= \mathbf{D}_k \mathbf{P} - \eta \left[(\mathbf{D}_k \mathbf{S}_{k+1} - \mathbf{X}) \mathbf{S}_{k+1}^T \mathbf{P} + \lambda \mathbf{D}_k (\mathbf{D}_k^T \mathbf{D}_k - \mathbf{I}) \mathbf{P} \right] \\ &= (\mathbf{D}_k - \eta \left[(\mathbf{D}_k \mathbf{S}_{k+1} - \mathbf{X}) \mathbf{S}_{k+1}^T + \lambda \mathbf{D}_k (\mathbf{D}_k^T \mathbf{D}_k - \mathbf{I}) \right]) \mathbf{P} \\ &= \mathbf{D}_{k+1} \mathbf{P} \end{aligned} \quad (10)$$

Thus, the result holds for $k + 1$, which completes the proof of the theorem.

This theorem demonstrates that the dictionary learning process preserves any fixed permutation \mathbf{P} applied to the initial dictionary. Based on this insight, we introduce a global alignment strategy that performs a one-time alignment of the initial dictionaries $\{\mathbf{D}_i^{(0)}\}_{i=1}^N$ across all sites by computing suitable permutation matrices relative to a chosen reference dictionary. Since subsequent updates preserve the permutation structure, all future dictionaries remain consistently aligned.

2.4 Global Alignment

To ensure consistent atom ordering across dictionaries from N sites, we performed a global alignment using the shortest path search [18]. Specifically, we construct a directed acyclic graph (DAG) with $N + 2$ layers, where each layer contains k nodes representing the dictionary atoms at each site. The edge weight between any two nodes in adjacent layers is defined as:

$$weight = \min(MSE(\mathbf{d}_i^j, \mathbf{d}_{i+1}^l), MSE(\mathbf{d}_i^j, -\mathbf{d}_{i+1}^l)), (i = 1, 2, \dots, N; j, l = 1, 2, \dots, k) \quad (11)$$

where $MSE(\cdot)$ denotes the mean squared error between two atoms. Intuitively, we want to pick the closest pairs of signed nodes $\pm \mathbf{d}_i^j, \pm \mathbf{d}_{i+1}^l$ from any consecutive layers.

We perform k rounds of the shortest path search to realize the global alignment. More concretely, in each round, we implement Dijkstra algorithm [19] to find the shortest weighted path from node s to node t from the current DAG, which is denoted as:

$$path = [s, (1, a_1), (2, a_2), \dots, (N, a_N), t] \quad (12)$$

where a_i indicates the selected atom index at site i . The selected atoms form the next aligned atom across all sites and are appended to the aligned dictionaries. We record their positions using signed permutation matrices to track the alignment. After each round, the selected nodes were removed from the DAG to avoid reselection, and the process was repeated until all k atoms were aligned. After k rounds, for each site i , the aligned dictionary \mathbf{D}_{A_i} satisfies the following:

$$\mathbf{D}_{A_i} = \mathbf{D}_i^{(0)} \mathbf{P}_i \quad (13)$$

where $\mathbf{D}_i^{(0)}$ is the original (pretrained) dictionary, and \mathbf{P}_i is a signed permutation matrix (each row and column contains one non-zero entry, either 1 or -1). The corresponding sparse representation matrices are updated as:

$$\{\mathbf{S}_{A_i}\}_{i=1}^N = \{\mathbf{P}_i^T \mathbf{S}_i^{(0)}\}_{i=1}^N \quad (14)$$

where \mathbf{P}_i^T denotes the transpose of the transformation matrix \mathbf{P}_i .

The pseudocode for the *Global Alignment* is presented in Algorithm 1.

Algorithm 1 Global Alignment

Require: Initial dictionaries $\{\mathbf{D}_i^{(0)}\}_{i=1}^N$, sparse codes $\{\mathbf{S}_i^{(0)}\}_{i=1}^N$, number of global atoms g

Ensure: Aligned dictionaries $\{\mathbf{D}_{A_i}\}_{i=1}^N$, updated sparse codes $\{\mathbf{S}_{A_i}\}_{i=1}^N$

- 1: Construct a DAG with $(N + 2)$ layers: source s , layers 1 to N , sink t
 - 2: Assign edge weights as minimum MSE over all signed atom pairs between adjacent layers
 - 3: **while** layers 1 to N are nonempty **do**
 - 4: Find shortest path from s to t using Dijkstra's algorithm
 - 5: Record sign of each selected atom on the path
 - 6: Update permutation-sign matrices $\{\mathbf{P}_i\}_{i=1}^N$
 - 7: Align selected atoms and append to \mathbf{D}_{A_i}
 - 8: Remove selected nodes from the DAG
 - 9: **end while**
 - 10: Obtain aligned dictionaries $\{\mathbf{D}_{A_i}\}_{i=1}^N$ and matrices $\{\mathbf{P}_i\}_{i=1}^N$
 - 11: Update sparse codes $\{\mathbf{S}_{A_i}\}_{i=1}^N$ via Eq.(14)
 - 12: **Return** $\{\mathbf{D}_{A_i}\}_{i=1}^N$ and $\{\mathbf{S}_{A_i}\}_{i=1}^N$
-

2.5 Federated Collaborative Regression

Based on the global alignment, Each aligned dictionary D_{A_i} at site i can be decomposed into global and local components

$$\{D_{A_i}\}_{i=1}^N = \left\{ \left(D_{A_i}^{\text{global}}, D_{A_i}^{\text{local}} \right) \right\}_{i=1}^N \quad (15)$$

Each site uploads its global component $D_{A_i}^{\text{global}}$ to the central server. The server then computes the global dictionary D_{avg} by performing a weighted average over all uploaded components:

$$D_{avg} = \sum_{i=1}^N \frac{n_i}{\sum_{i=1}^N n_i} D_{A_i}^{\text{global}} \quad (16)$$

where n_i denotes the number of samples at site i . The server then broadcasts the aggregated global dictionary D_{avg} back to all participating sites. Each site replaces its local version of the global dictionary $D_{A_i}^{\text{global}}$ with the updated D_{avg} , resulting in the final personalized dictionary:

$$\{D'_i\}_{i=1}^N = \left\{ \left(D_{avg}, D_{A_i}^{\text{local}} \right) \right\}_{i=1}^N \quad (17)$$

Building upon the federated dictionary learning framework, we introduce federated collaborative regression, which jointly optimizes both reconstruction and supervised learning objectives. This enables the model to learn feature representations that are not only compact and expressive but also discriminative with respect to the target labels.

To extend this supervised learning framework to a federated setting, we allow each client to learn both shared and personalized components of the dictionary while collaboratively updating the global model. Specifically, each client independently optimizes its local variables (D_i, S_i, w_i) , where $D_i = [D_i^{\text{global}}, D_i^{\text{local}}]$, and participates in federated aggregation using only the global dictionary component and the model parameters. The resulting federated optimization problem is defined as:

$$\min_{D_i, S_i, w_i} \sum_{i=1}^N L(Y_i, S_i, w_i) + \lambda_1 \|X_i - D_i S_i\|_F^2 + \lambda_2 \|S_i\|_1 + \lambda_3 \|w_i\|_2^2 + \lambda_4 \|D_i D_i^T - I\|_F^2 \quad (18)$$

where $L(Y, S, w)$ denotes the loss function of the classification task, the term $\lambda_3 \|w\|_2^2$ is included to prevent overfitting in the classification process, and $\lambda_4 \|D D^T - I\|_F^2$ represents the orthogonality constraint imposed on the dictionary D .

The pseudocode for the PFedDL framework is detailed in Algorithm 2

3 Experiments and Results

3.1 Data Acquisition

To evaluate the effectiveness of the proposed method, we conducted experiments on the publicly available multi-site dataset ABIDE [20]. This dataset compiles brain neuroimaging data from multiple institutions to enhance our understanding of the neural mechanisms underlying Autism Spectrum Disorder (ASD).

In this study, we selected resting-state fMRI data from four data collection sites within ABIDE: UM_1, NYU, USM, and UCLA_1. Together, these sites provide data from 370 subjects, including both individuals with ASD and neurotypical controls (NC). Specifically, NYU contains 167 subjects (73 with ASD and 94 NC); UCLA_1 includes 63 subjects (37 ASD, 26 NC); UM_1 comprises 88 subjects (43 ASD, 45 NC); and USM includes 52 subjects (33 ASD, 19 NC).

3.2 Data Preprocessing

The raw resting-state fMRI data from the ABIDE dataset were pre-processed using the CPAC pipeline proposed by Craddock et al. [21], as shown in Figure 2. The preprocessing steps included band-pass filtering in the frequency range of 0.01 to 0.1 Hz, without performing global signal regression. The

Algorithm 2 PFedDL

Require: Local datasets \mathbf{X}_i and labels \mathbf{Y}_i for each client $i = 1, \dots, N$
Require: Hyperparameter: $\lambda_1, \lambda_2, \lambda_3, \lambda_4$, learning rate η , dictionary size k , global dictionary size g , local steps $\text{iters}_{\text{local}}$, federated rounds $\text{iters}_{\text{Fed}}$
Ensure: Classifier parameters \mathbf{w}_i , learned dictionaries \mathbf{D}_i , sparse codes \mathbf{S}_i

- 1: **for** each client $i = 1$ to N **in parallel do**
- 2: Perform traditional dictionary learning on $(\mathbf{X}_i, \mathbf{Y}_i)$
- 3: Obtain initial $\mathbf{D}_i^{(0)}, \mathbf{S}_i^{(0)}$
- 4: **end for**
- 5: $\{\mathbf{D}_{A_i}\}_{i=1}^N, \{\mathbf{S}_{A_i}\}_{i=1}^N = \text{GlobalAlignment}(\{\mathbf{D}_i^{(0)}\}_{i=1}^N, \{\mathbf{S}_i^{(0)}\}_{i=1}^N)$
- 6: **for** iter = 1 to $\text{iters}_{\text{Fed}}$ **do**
- 7: **for** each client $i = 1$ to N **in parallel do**
- 8: **for** it = 1 to $\text{iters}_{\text{local}}$ **do**
- 9: **Update classifier parameters:**
- 10: $\mathbf{w}_i \leftarrow \mathbf{w}_i - \eta \left(\frac{\partial L(\mathbf{Y}_i, \mathbf{S}_i, \mathbf{w}_i)}{\partial \mathbf{w}_i} + \lambda_3 \mathbf{w}_i \right)$
- 11: **Update sparse codes:**
- 12: $\mathbf{S}_i \leftarrow \text{SoftThreshold} \left(\mathbf{S}_i - \eta \left(\frac{\partial L(\mathbf{Y}_i, \mathbf{S}_i, \mathbf{w}_i)}{\partial \mathbf{S}_i} + \lambda_1 \mathbf{D}_i^T (\mathbf{D}_i \mathbf{S}_i - \mathbf{X}_i) \right), \eta \lambda_2 \right)$
- 13: **Update dictionary:**
- 14: $\mathbf{D}_i \leftarrow \mathbf{D}_i - \eta \left(\lambda_1 (\mathbf{D}_i \mathbf{S}_i - \mathbf{X}_i) \mathbf{S}_i^T + \lambda_4 \mathbf{D}_i (\mathbf{D}_i^T \mathbf{D}_i - \mathbf{I}) \right)$
- 15: **Normalize \mathbf{D}_i**
- 16: **Send** global dictionary component $\mathbf{D}_i^{\text{global}}$ to server
- 17: **end for**
- 18: **end for**
- 19: **Server: Compute global average**
- 20: $\mathbf{D}_{\text{avg}} = \sum_{i=1}^N \frac{n_i}{\sum_{i=1}^N n_i} \mathbf{D}_i^{\text{global}}$
- 21: **Server: Broadcast \mathbf{D}_{avg} to all clients**
- 22: **for** each client $i = 1$ to N **do**
- 23: $\mathbf{D}_i = [\mathbf{D}_{\text{avg}}, \mathbf{D}_i^{\text{local}}]$
- 24: **end for**
- 25: **end for**
- 26: **Return** $\{\mathbf{w}_i, \mathbf{D}_i, \mathbf{S}_i\}_{i=1}^N$

preprocessed fMRI data were then segmented into 111 regions of interest (ROIs) based on the Harvard-Oxford (HO) brain atlas [22]. For each participant, we extracted ROI time series and computed pairwise Pearson correlations, yielding a symmetric 111×111 functional-connectivity matrix that was z-standardized with Fisher's transformation to improve normality [23]. Given that these matrices are symmetric with diagonal elements equal to one, we retained only the lower triangular part (excluding the diagonal) and vectorized it to obtain a feature vector $\mathbf{v}_a \in R^{6105}$ for subject a. For each site i, the feature vectors of all subjects n_i were concatenated column-wise to form the site-specific data matrix $\mathbf{X}_i = [\mathbf{v}_1, \mathbf{v}_2, \dots, \mathbf{v}_{n_i}] \in R^{6105 \times n_i}$. In this study, binary labels were assigned to indicate diagnostic status: ASD was labeled as 1, and NC as 0.

3.3 Experimental Setup

The experiments were carried out using the PyTorch framework on a system equipped with an NVIDIA GeForce RTX 4080 GPU. In addition to conventional machine learning methods such as random forest (RF) [24][25] and support vector machine (SVM) [26][27], we compared our approach with several deep learning baselines, particularly graph neural network (GNN) architectures commonly used in functional connectivity analysis, including GCN [28], GAT [29] and BrainGNN [30].

To determine an appropriate dictionary size, we evaluated a range of values for k from 10 to 1400 (Figure 3). Based on the trade-off between computational efficiency and classification performance, we selected $k = 400$ as the optimal configuration. Following optimization through grid search, the hyperparameters were set to $\lambda_1 = 1, \lambda_2 = 0.005, \lambda_3 = 1.5, \lambda_4 = 0.01, \eta = 0.0001$, with $\eta = 0.0001$ and $g = 370$.

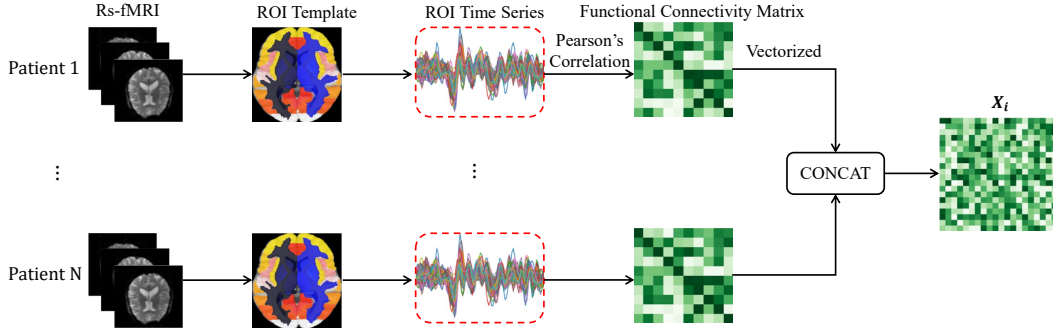


Figure 2: Flowchart of the data preprocessing procedure

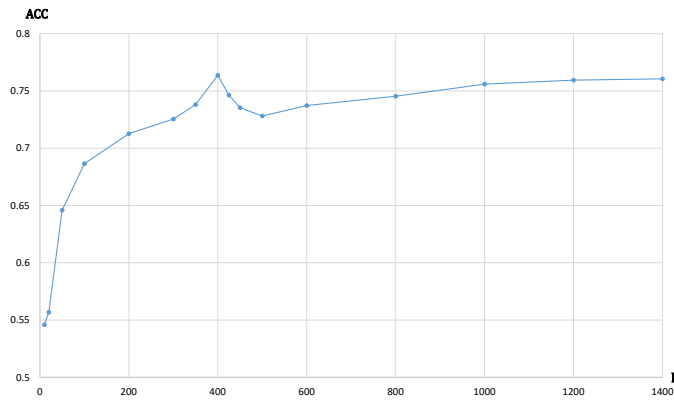


Figure 3: Model Sensitivity to Dictionary Size k .

3.4 Result

The average classification accuracies from four-fold cross-validation are summarized in Table 1. PFedDL outperforms all baselines at every site (NYU, UCLA_1, UM_1, and USM) as well as in terms of average classification accuracy. It achieves an average accuracy of 76.4%, significantly surpassing traditional machine learning methods (RF: 60.2%, SVM: 61.5%), graph neural networks (GCN: 64.44%, GAT: 70.1%), and even the more advanced BrainGNN model (73.7%).

Table 1: Comparison of classification accuracy on the ABIDE dataset

Site / Model	NYU	UCLA_1	UM_1	USM	Average
MLP	0.589 ± 0.031	0.546 ± 0.029	0.563 ± 0.034	0.689 ± 0.033	0.597
GCN	0.621 ± 0.029	0.645 ± 0.031	0.594 ± 0.032	0.716 ± 0.029	0.644
GAT	0.668 ± 0.028	0.699 ± 0.027	0.685 ± 0.028	0.749 ± 0.026	0.701
BrainGNN	0.667 ± 0.034	0.753 ± 0.025	0.711 ± 0.037	0.818 ± 0.026	0.737
RF	0.577 ± 0.031	0.602 ± 0.052	0.591 ± 0.043	0.637 ± 0.023	0.602
SVM	0.593 ± 0.021	0.587 ± 0.036	0.626 ± 0.031	0.655 ± 0.021	0.615
PFedDL	0.671 ± 0.028	0.745 ± 0.031	0.716 ± 0.029	0.923 ± 0.032	0.764

Performance at the USM site is particularly impressive, with PFedDL achieving 92.3% accuracy, 12.8% higher than the second best model, BrainGNN (81.8%). Notably, the USM site consistently yields strong results across all models, suggesting a higher signal-to-noise ratio or more distinct pathological features in its data.

In contrast, the NYU site, despite having the largest sample size and the greatest influence in federated averaging, shows the lowest performance across all models. This may be due to higher data noise or substantial variability in imaging acquisition equipment or conditions compared to the other sites.

3.5 Significance Results

To identify ROI highly associated with disease, we conducted an analysis based on dictionary learning results. Using the model parameters w_i , we selected the top 10 dictionary atoms with the highest discriminative power. These atoms were projected back to the original functional connectivity space from the sparse feature space. Each atom corresponds to the vectorized upper triangular portion of a connectivity matrix, which was reshaped to recover the associated connectivity pattern.

To evaluate the importance of each ROI, we calculated the total connection strength involving each ROI in the reconstructed connectivity matrices, weighted by the corresponding weights w_i , and summed across all selected atoms to obtain a global importance score. The top 10 ROIs with the highest scores were identified as key areas potentially associated with disease-related functional brain regions.

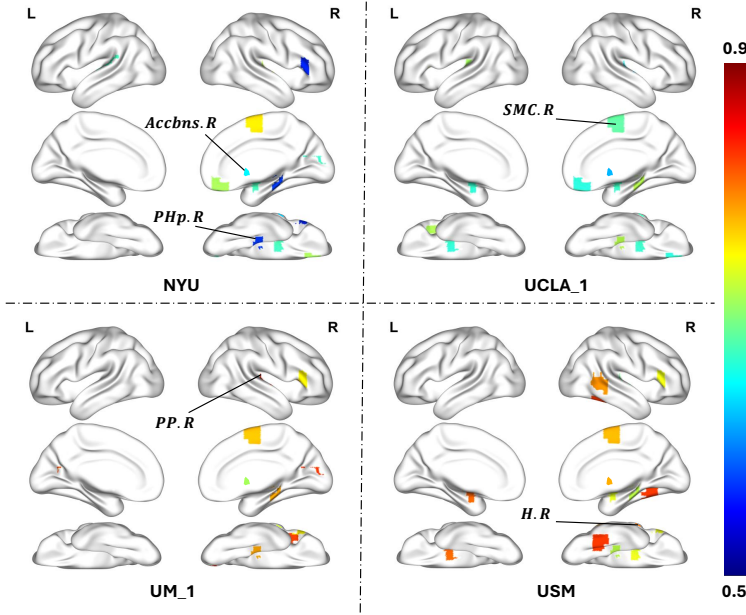


Figure 4: Discriminative Brain Regions Highlighted by PFedDL for ASD.

We visualized the identified ROIs using BrainNet Viewer [31], projecting them onto the cortical surface in standard MNI space. As shown in Figure 4, our method consistently highlighted representative brain regions implicated in the ASD vs. NC classification task across the four sites. Notably, five functional regions were consistently selected across all sites: the right accumbens (Accbns.R), right juxtapositional lobule cortex (SMC.R), right parahippocampal gyrus (PHp.R), right planum polare (PP.R), and right Heschl’s gyrus (H.R). These regions have been previously reported in the literature as being implicated in ASD-related neural alterations [32][33][34][35].

It should also be noted that the ROI importance scores at the NYU site were significantly lower than those at the other sites, whereas the USM site exhibited the highest scores. This pattern is consistent with the classification performance at each site, reflecting the varying signal quality or disease-related heterogeneity across sites.

4 Conclusion

This paper presents PFedDL, a novel personalized federated dictionary learning framework designed to address data heterogeneity and privacy concerns in multi-site brain imaging analysis. By incor-

porating global-local dictionary decomposition and a global alignment mechanism within an FL framework, PFedDL enables personalized modeling while retaining the collaborative advantages of federated training. Experiments on the ABIDE dataset demonstrate that PFedDL consistently outperforms widely used machine learning methods and state-of-the-art deep learning approaches across multiple sites.

Despite promising results, PFedDL has several limitations. Despite promising results, PFedDL has several limitations. One notable constraint is the limited size of the dataset, as the total number of subjects in the four sites is only 370. Moreover, the current framework is limited to static connectivity analysis. Future work will focus on improving scalability to handle larger, high-dimensional, and multi-modal datasets, and on extending the framework to dynamic brain networks. We hope that this study encourages research at the intersection of federated learning, representation learning, and neuroimaging, particularly toward the development of privacy-preserving and generalizable models for biomedical data analysis.

References

- [1] Cornelis J Stam. Modern network science of neurological disorders. *Nature Reviews Neuroscience*, 15(10):683–695, 2014.
- [2] Yuhui Du, Zening Fu, and Vince D Calhoun. Classification and prediction of brain disorders using functional connectivity: promising but challenging. *Frontiers in neuroscience*, 12:525, 2018.
- [3] Thomas F Varley, Michael Craig, Ram Adapa, Paola Finoia, Guy Williams, Judith Allanson, John Pickard, David K Menon, and Emmanuel A Stamatakis. Fractal dimension of cortical functional connectivity networks & severity of disorders of consciousness. *PloS one*, 15(2):e0223812, 2020.
- [4] Brendan McMahan, Eider Moore, Daniel Ramage, Seth Hampson, and Blaise Aguerre y Arcas. Communication-efficient learning of deep networks from decentralized data. In *Artificial intelligence and statistics*, pages 1273–1282. PMLR, 2017.
- [5] Tian Li, Anit Kumar Sahu, Ameet Talwalkar, and Virginia Smith. Federated learning: Challenges, methods, and future directions. *IEEE signal processing magazine*, 37(3):50–60, 2020.
- [6] Xiaoxiao Li, Yufeng Gu, Nicha Dvornek, Lawrence H Staib, Pamela Ventola, and James S Duncan. Multi-site fmri analysis using privacy-preserving federated learning and domain adaptation: Abide results. *Medical image analysis*, 65:101765, 2020.
- [7] Xingchao Peng, Zijun Huang, Yizhe Zhu, and Kate Saenko. Federated adversarial domain adaptation. *arXiv preprint arXiv:1911.02054*, 2019.
- [8] Rui Jin, Krishna K Dontaraju, Seung-Jun Kim, Mohammad Abu Baker Siddique Akhonda, and Tülay Adalı. Dictionary learning-based fmri data analysis for capturing common and individual neural activation maps. *IEEE Journal of Selected Topics in Signal Processing*, 14(6):1265–1279, 2020.
- [9] Biao Cai, Gemeng Zhang, Wenxing Hu, Aiyong Zhang, Pascal Zille, Yipu Zhang, Julia M Stephen, Tony W Wilson, Vince D Calhoun, and Yu-Ping Wang. Refined measure of functional connectomes for improved identifiability and prediction. *Human brain mapping*, 40(16):4843–4858, 2019.
- [10] Peter Kairouz, H Brendan McMahan, Brendan Avent, Aurélien Bellet, Mehdi Bennis, Arjun Nitin Bhagoji, Kallista Bonawitz, Zachary Charles, Graham Cormode, Rachel Cummings, et al. Advances and open problems in federated learning. *Foundations and trends® in machine learning*, 14(1–2):1–210, 2021.
- [11] Ron Rubinfeld, Alfred M Bruckstein, and Michael Elad. Dictionaries for sparse representation modeling. *Proceedings of the IEEE*, 98(6):1045–1057, 2010.
- [12] Ivana Tošić and Pascal Frossard. Dictionary learning. *IEEE Signal Processing Magazine*, 28(2):27–38, 2011.

- [13] Monica Fira, Hariton-Nicolae Costin, and Liviu Goras. A study on dictionary selection in compressive sensing for ecg signals compression and classification. *Biosensors*, 12(3):146, 2022.
- [14] Jirayu Samkunta, Patinya Ketthong, Nghia Thi Mai, Md Abdus Samad Kamal, Iwanori Murakami, and Kou Yamada. Feature extraction based on sparse coding approach for hand grasp type classification. *Algorithms*, 17(6):240, 2024.
- [15] Qixin Chen, Hongye Guo, Kedi Zheng, Yi Wang, Qixin Chen, Hongye Guo, Kedi Zheng, and Yi Wang. Subspace characteristics of Imp data. *Data Analytics in Power Markets*, pages 91–112, 2021.
- [16] Fangyuan Gao, Xin Deng, Mai Xu, Jingyi Xu, and Pier Luigi Dragotti. Multi-modal convolutional dictionary learning. *IEEE Transactions on Image Processing*, 31:1325–1339, 2022.
- [17] Qiushi Huang, Wenqian Jiang, Jian Shi, Chenye Wu, Dan Wang, and Zhu Han. Federated shift-invariant dictionary learning enabled distributed user profiling. *IEEE Transactions on Power Systems*, 39(2):4164–4178, 2023.
- [18] Keke Huang, Xinyi Liu, Fanbiao Li, Chunhua Yang, Okyay Kaynak, and Tingwen Huang. A federated dictionary learning method for process monitoring with industrial applications. *IEEE Transactions on Artificial Intelligence*, 4(5):1017–1028, 2022.
- [19] Edsger W Dijkstra. A note on two problems in connexion with graphs. In *Edsger Wybe Dijkstra: his life, work, and legacy*, pages 287–290. 2022.
- [20] Adriana Di Martino, Chao-Gan Yan, Qingyang Li, Erin Denio, Francisco X Castellanos, Kaat Alaerts, Jeffrey S Anderson, Michal Assaf, Susan Y Bookheimer, Mirella Dapretto, et al. The autism brain imaging data exchange: towards a large-scale evaluation of the intrinsic brain architecture in autism. *Molecular psychiatry*, 19(6):659–667, 2014.
- [21] Cameron Craddock, Yassine Benhajali, Carlton Chu, Francois Chouinard, Alan Evans, András Jakab, Budhachandra Singh Khundrakpam, John David Lewis, Qingyang Li, Michael Milham, et al. The neuro bureau preprocessing initiative: open sharing of preprocessed neuroimaging data and derivatives. *Frontiers in Neuroinformatics*, 7(27):5, 2013.
- [22] Rahul S Desikan, Florent Ségonne, Bruce Fischl, Brian T Quinn, Bradford C Dickerson, Deborah Blacker, Randy L Buckner, Anders M Dale, R Paul Maguire, Bradley T Hyman, et al. An automated labeling system for subdividing the human cerebral cortex on mri scans into gyral based regions of interest. *Neuroimage*, 31(3):968–980, 2006.
- [23] Xi Yang, Yan Jin, Xiaobo Chen, Han Zhang, Gang Li, and Dinggang Shen. Functional connectivity network fusion with dynamic thresholding for mci diagnosis. In *Machine Learning in Medical Imaging: 7th International Workshop, MLMI 2016, Held in Conjunction with MICCAI 2016, Athens, Greece, October 17, 2016, Proceedings 7*, pages 246–253. Springer, 2016.
- [24] Steven J Rigatti. Random forest. *Journal of Insurance Medicine*, 47(1):31–39, 2017.
- [25] Leo Breiman. Random forests. *Machine learning*, 45:5–32, 2001.
- [26] Marti A. Hearst, Susan T Dumais, Edgar Osuna, John Platt, and Bernhard Scholkopf. Support vector machines. *IEEE Intelligent Systems and their applications*, 13(4):18–28, 1998.
- [27] Shan Suthaharan. Support vector machine. In *Machine learning models and algorithms for big data classification: thinking with examples for effective learning*, pages 207–235. Springer, 2016.
- [28] Thomas N Kipf and Max Welling. Semi-supervised classification with graph convolutional networks. *arXiv preprint arXiv:1609.02907*, 2016.
- [29] Petar Velickovic, Guillem Cucurull, Arantxa Casanova, Adriana Romero, Pietro Lio, Yoshua Bengio, et al. Graph attention networks. *stat*, 1050(20):10–48550, 2017.

- [30] Xiaoxiao Li, Yuan Zhou, Nicha Dvornek, Muhan Zhang, Siyuan Gao, Juntang Zhuang, Dustin Scheinost, Lawrence H Staib, Pamela Ventola, and James S Duncan. Braingnn: Interpretable brain graph neural network for fmri analysis. *Medical Image Analysis*, 74:102233, 2021.
- [31] Mingrui Xia, Jinhui Wang, and Yong He. Brainnet viewer: a network visualization tool for human brain connectomics. *PloS one*, 8(7):e68910, 2013.
- [32] Charlems Alvarez-Jimenez, Nicolás Múnera-Garzón, Maria A Zuluaga, Nelson F Velasco, and Eduardo Romero. Autism spectrum disorder characterization in children by capturing local-regional brain changes in mri. *Medical physics*, 47(1):119–131, 2020.
- [33] Wonsik Jung, Eunjin Jeon, Eunsong Kang, and Heung-II Suk. Eag-rs: A novel explainability-guided roi-selection framework for asd diagnosis via inter-regional relation learning. *IEEE Transactions on Medical Imaging*, 43(4):1400–1411, 2023.
- [34] Hildegard Janouschek, Henry W Chase, Rachel J Sharkey, Zeru J Peterson, Julia A Camilleri, Ted Abel, Simon B Eickhoff, and Thomas Nickl-Jockschat. The functional neural architecture of dysfunctional reward processing in autism. *NeuroImage: Clinical*, 31:102700, 2021.
- [35] Daegyeom Kim, Joo Young Lee, Byeong Chang Jeong, Ja-Hye Ahn, Johanna Inhyang Kim, Eun Soo Lee, Hyuna Kim, Hyun Ju Lee, and Cheol E Han. Overconnectivity of the right heschl’s and inferior temporal gyrus correlates with symptom severity in preschoolers with autism spectrum disorder. *Autism Research*, 14(11):2314–2329, 2021.